Click Here for Full Article

Paleointensity record from the 2.7 Ga Stillwater Complex, Montana

P. A. Selkin

Environmental Science Program, Interdisciplinary Arts and Sciences, University of Washington, Tacoma, Washington 98402, USA (paselkin@u.washington.edu)

J. S. Gee

Scripps Institution of Oceanography, University of California, San Diego, La Jolla, California 92093, USA

W. P. Meurer

Improved Hydrocarbon Recovery Division, ExxonMobil Upstream Research Company, P. O. Box 2189, Houston, Texas 77252-2189, USA

S. R. Hemming

Lamont–Doherty Earth Observatory, Route 9W, Palisades, New York 10964, USA

[1] The record of geomagnetic intensity captured in the 2.7 Ga Stillwater Complex (Montana, USA) provides a statistical description of the Archean geodynamo. We present results of modified Thellier paleointensity experiments on 441 core specimens, 114 of which pass strict reliability criteria. The specimens are from 53 sites spanning most of the Banded Series rocks in the Stillwater Complex. On the basis of thermochronologic and petrologic evidence, we interpret the highest temperature component of remanence to be a late Archean thermoremanence, though the possibility remains that it is a thermochemical remanence. Thermal models indicate that the highest temperature magnetization component at each of the sites averages $\sim$20–200 ka of geomagnetic secular variation. The suite of sites as distributed through the Banded Series samples a roughly a 1 Ma time interval. The average of the most reliable paleointensity measurements, uncorrected for the effects of anisotropy or cooling rate, is 38.2 ± 11.3 μT (1σ). Remanence anisotropy, cooling rate, and the nonlinear relationship between applied field and thermoremanence have a significant effect on paleointensity results; a corrected average of 30.6 ± 8.8 μT is likely a more appropriate value. Earth's average dipole moment during the late Archean (5.05 ± 1.46 × 10^{22} Am^2, λ_{pmag} = 44.5°) was well within the range of estimates from Phanerozoic rocks. The distribution of site-mean paleointensities around the mean is consistent with that expected from slow cooling over timescales expected from thermal models and with secular variation comparable to that of the Phanerozoic field.

1. Introduction

[2] The geomagnetic field is one of the few indicators of deep-earth behavior that is measurable at the Earth's surface and is recorded by geological processes. As such, records of the Earth's ancient magnetic field are extremely valuable in tracing the geodynamo's behavior early in Earth's history. Models suggest that paleomagnetic (directional and intensity) records can provide information on inner core growth [*Buffett*, 2002, 2003; *Coe and Glatzmaier*, 2006; *Gubbins et al.*, 2003; *Hollerbach and Jones*, 1993; *Labrosse and Macouin*, 2003; *Stevenson*, 2003] and are among the few constraints on the energy budget of the core [*Costin and Butler*, 2006; *Glatzmaier et al.*, 1999]. Therefore, the early Earth's magnetic field has been a subject of intense study, especially over the past decade (see review in the work of *Dunlop and Yu* [2004]).

[3] Paleomagnetic studies have demonstrated that the geodynamo was active during the Archean, with documented polarity reversals (and possibly superchrons) as early as 2.7 Ga [*Strik et al.*, 2003]. Directional paleomagnetic records from 2.5 to 2.7 Ga rocks [*Biggin et al.*, 2008] and geodynamo simulations [*Coe and Glatzmaier*, 2006] may indicate a stable geodynamo during the late Archean, with reduced paleosecular variation compared to the past 5 Ma. In contrast, Archean intensity estimates [*Tarduno et al.*, 2006] and a subset of the 2.5–2.7 Ga directional data [*Smirnov and Tarduno*, 2004] have been interpreted as reflecting geomagnetic field behavior similar to that of the past 5 Ma. Measurements of the intensity of Earth's magnetic field (paleointensity) from deep geologic time can, in principle, test the link between inner core growth and geodynamo behavior. Though successful paleointensity measurements have been made on Archean rocks (see section 6), reliable paleomagnetic records from the Archean, the first 2 billion years of Earth's existence, are sparse.

[4] The 2.7 Ga Stillwater Complex (Montana, USA; see review in the work of *McCallum* [1996]) contains anorthositic, gabbroic, and ultramafic rocks that are good candidates for paleomagnetic studies of the Archean for several reasons. Geochronologic data indicate that both the formation and the cooling of the Stillwater Complex took place during the late Archean (Table 1; see review in the work of *Lambert et al.* [1985]). Hornblende Ar/Ar ages presented here (see section 3.5) are consistent with no significant reheating (>550°C) since the latest Archean.

[5] Stillwater Complex rocks, primarily those with abundant plagioclase, carry a high-stability component of remanence, interpreted to be a TRM acquired as the rocks initially cooled [*Bergh*, 1970; *Xu et al.*, 1997]. A modified contact test indicated that some Stillwater Complex rocks had been locally remagnetized after their initial cooling but that the high-temperature component of remanence is unlikely to be associated with later Precambrian dikes that crosscut the complex [*Xu et al.*, 1997]. The high-stability component of remanence is associated with fine-grained magnetite present as elongate particles in plagioclase [*Geissman et al.*, 1988; *Selkin et al.*, 2000; *Xu et al.*, 1997]. Rocks from the Stillwater Complex are likely to yield reliable paleointensity estimates and have done so in previous studies [*Bergh*, 1970; *Selkin et al.*, 2000]. However, paleointensity studies have changed considerably since the early 1970s. Improved consistency checks and greater understanding of rock-magnetic effects have enhanced our ability to interpret paleointensity results and to distinguish more reliable records from less reliable ones.

2. Sampling

[6] In conjunction with a fabric study [*Gee et al.*, 2004], we collected 988 oriented cores along with 45 oriented block samples at 515 sites within five localities on the East Boulder Plateau (Figure 1, Table S1 in the auxiliary material).[1] We supplemented these cores with subsamples of diamond drill cores from the Stillwater Mining Company's Nye and East Boulder adits, which we consider a sixth sampling locality (SMC). In the context of this study, a site consists of a set of cores (typically two) drilled at about the same stratigraphic horizon. Each core was cut into several (typically five) 1-inch specimens.

[7] There is considerable overlap between the stratigraphic intervals sampled at the different localities (Figure 2). In particular, we focused our sampling in multiple localities on approximately the same interval of the Middle and Upper Banded Series.

[8] Orientations of the field-drilled cores were determined using both magnetic and sun compass. SMC specimens were marked according to drill direction, and then oriented using a method based on anisotropy of magnetic susceptibility (Figure 3). For most lithologies in the Stillwater, the minimum

---

Table 1. Summary of Representative Stillwater Complex Age Data, As Reported in Original References[a]

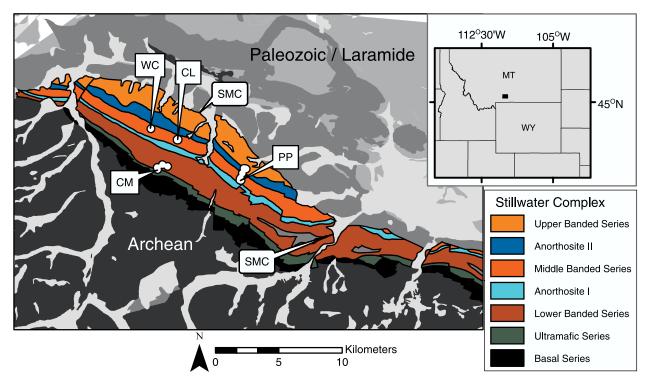| Isotope System	Age (Ma)	Reference
K-Ar (Plagioclase)	2000–3200	[*Kistler et al.*, 1969]
K-Ar (Phlogopite)	2540–2640	[*Kistler et al.*, 1969]
Rb-Sr (Whole Rock)	2108–2608	[*Fenton and Faure*, 1969]
Rb-Sr (Whole Rock)*	2522–2822	[*Powell et al.*, 1969]
Rb-Sr (Whole Rock)*	2647–2737	[*Mueller and Wooden*, 1976]
Sm-Nd (Whole Rock, Plagioclase, Bronzite, Augite)	2693–2709	[*DePaolo and Wasserburg*, 1979]
Sm-Nd (Whole Rock)	2862–2930	[*Tatsumoto and Coffrant*, 1980]
Sm-Nd (Whole Rock)	2708–2776	[*Tatsumoto and Coffrant*, 1980]
Sm-Nd (Whole Rock)	2782–2814	[*Tatsumoto and Coffrant*, 1980]
U-Pb (Zircon)	2700–2750	[*Nunes and Tilton*, 1971]
Pb-Pb (Whole Rock)	2650–2674	[*Manhes et al.*, 1980]
U-Pb (Zircon)	2596–2770	[*Lambert et al.*, 1985]
U-Pb (Zircon, Baddeleyite)	2701–2709	[*Premo et al.*, 1990]
Re-Os (Chromitite)	2660–2820	[*Marcantonio et al.*, 1993]

[a] Asterisk indicates ages of metasedimentary rocks in Stillwater contact aureole.

principal axis of anisotropy of magnetic suscepti-bility (AMS, measured on Kappabridge KLY-2) is a good proxy for the normal to magmatic foliation [*Gee et al.*, 2004], which is approximately parallel to igneous layering. Mine cores with a well-developed AMS foliation were rotated about the drill direction so that the AMS minima aligned with the normal to the mean foliation measured from outcrops. The reorientation technique does not work well for most anorthositic horizons, which have weak (and in some cases inverse) AMS fabrics.
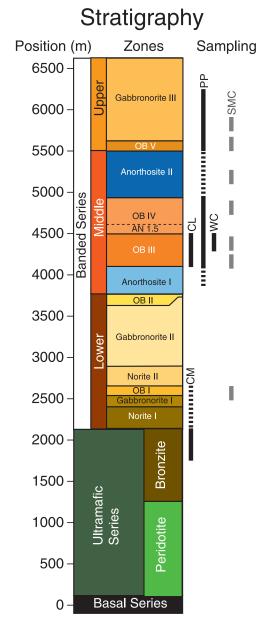
3. Pilot Studies

3.1. Paleomagnetism

[9] We carried out a pilot paleomagnetic study to identify the characteristic component of rema-

Figure 1. Generalized geologic map of the Stillwater Complex and surrounding areas [*Page et al.*, 2002; *Raines and Johnson*, 1995] showing sampling locations. East Boulder Plateau sites (see Table S1 in the auxiliary material) in square balloons. PP is Picket Pin Mountain. CM is Chrome Mountain. CL is Camp Lake. WC is Western Contact Mountain. Stillwater Mining Company (SMC) sites in rounded balloons.

Figure 2. Stratigraphic column of the Stillwater Complex [after *McCallum*, 1996] showing extent of sampling at different localities. Locality designations as in Figure 1. Dotted lines indicate areas of relatively sparse sampling. OB is olivine-bearing. AN is Anorthosite.

nence, to identify sites affected by lightning, and to select specimens for paleointensity experiments. Specimens from approximately every other site in the Picket Pin (PP), Western Contact Mtn. (WC), and Chrome Mtn. (CM) sections, from many sites from the Camp Lake (CL) section, and from several SMC cores were thermally demagnetized. We heated specimens in computer controlled ovens in the Scripps Paleomagnetic Facility that allow the heating of samples in $5° \pm 1°C$ temperature steps.

Several dozen specimens were also demagnetized in alternating fields (AF) using a Sapphire Instruments SI-4 demagnetizer. Above 80 mT, samples were demagnetized in a set of directions designed to counteract gyroremanent magnetization (The "Zijderveld-Dunlop" method of *Stephenson* [1993]). In most cases, the maximum peak alternating field used was 180 mT, although some samples were almost completely demagnetized (below 1% of NRM) at lower peak fields (typically 80–120 mT).
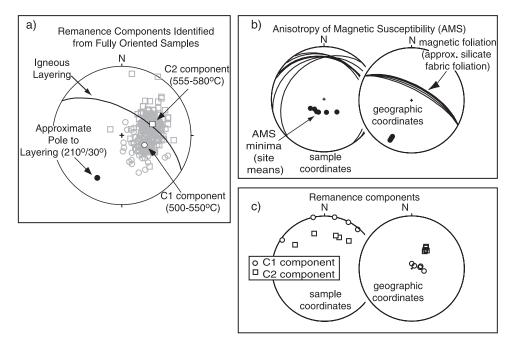
[10] Two end-member types of unblocking temperature and AF demagnetization behavior (Figure 4) characterize the Stillwater specimens. Plagioclase-rich rocks, characterized by susceptibilities on the order of 100 μSI or less, typically have discrete, high laboratory unblocking temperatures about 550–580°C (e.g., Figure 4a; n = 58 thermally demagnetized specimens). These specimens, or sister specimens from the same drill core, generally also have high median destructive fields (MDFs), above 60 mT (e.g., Figure 4b; n = 102 AF demagnetized specimens). Rocks of this type are common in the upper sections of the complex, particularly the Upper Banded Series. Gabbroic rocks (susceptibility on the order of 1000 μSI or more), which are common in the lower sections of the complex, have a discrete but lower range of unblocking temperatures (approximately 500–550°C; e.g., Figure 4c; n = 84), and lower MDFs (30–40 mT: e.g., Figure 4d; n = 36) than do the plagioclase-rich rocks. Most specimens fall into one of these two groups, although a significant fraction of specimens from the pilot study have a more distributed range of lower unblocking temperatures (Figures 4e–4f; n = 90 thermal, 89 AF).

3.2. Remanence Directions

[11] Stillwater specimens have up to three magnetization components with distinct directions and unblocking temperature ranges (C0, C1, and C2 in Figure 5). Not all components were observed in all specimens. No present-field overprint has been identified in the samples in the pilot study. The remanence directions discussed here are mean directions in stratigraphic coordinates (mean foliation, 304/57°, tilted to horizontal about strike; other coordinate systems in Table 2) and have been corrected for the effects of anisotropy [*Cogné*, 1987; *Hyodo and Dunlop*, 1993], unless otherwise noted.

[12] The lowest-temperature component, C0, is removed by thermal demagnetization up to about
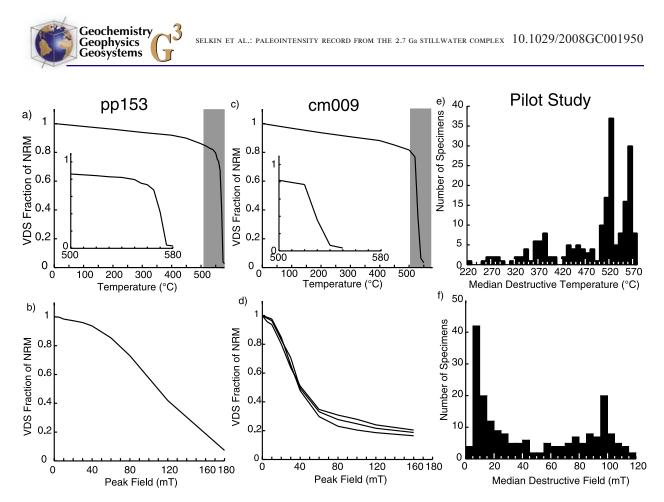
Figure 3. Reorientation of Stillwater Mining Company (SMC) cores using anisotropy of magnetic susceptibility (AMS). All plots are equal area projections in geographic coordinates and show data prior to anisotropy correction. Filled symbols indicate lower hemisphere projections; open symbols indicate upper hemisphere. (a) Orientation of igneous layering and remanence components C1 and C2 from fully oriented samples (see section 3). (b) Left side shows orientation of AMS minima (circles) and magnetic foliation (planes perpendicular to AMS minima; great circles) as measured in SMC cores. Right side shows rotation about drill core axis brings AMS minima into coincidence with each other, and AMS foliations into approximate coincidence with igneous layering. (c) Left side shows orientation of C1 and C2 before rotation in Figure 3b. Right side shows after rotation in Figure 3b.

$450–500°C$. The orientation of C0 varies considerably from site to site, although its direction is consistent within each site (Figures 5a and 5c). The directional variability in the C0 component may be the result of local reheating by dikes: the mean C0 direction ($323/27°$ in geographic coordinates; $\kappa = 2.8$; $N = 52$; $\alpha_{95} = 11.6°$; not corrected for remanence anisotropy) is broadly similar to that of a Precambrian dike sampled by Saxton ($323/55°$ reported by *Xu et al.* [1997]), though given the variability in the C0 direction, this may be a coincidence.

[13] The C1 and C2 components unblock at higher temperatures. C1 has unblocking temperatures between 500 and $550°C$. This component is typically distinct in thermal but not in AF demagnetization (Figure 5a), and has a mean direction of $175/−33°$ ($\kappa = 8$; $N = 96$; $\alpha_{95} = 5.1°$; Figure 6a). The C1 component is not present in all specimens (e.g., Figures 5d–5e), and is the only component resolved in others, particularly in the Lower and Middle Banded Series (Figures 5b, 5c, and 5f). Most of the specimens that have retained only a C1 component are pyroxene-rich mafic or ultramafic rocks. C2 is sometimes accompanied by C0 and/or

C1 (Figures 5a and 5e) but occasionally is the only resolvable magnetization component, especially in high-coercivity (MDF > 60 mT), high-unblocking-temperature rocks of the Upper Banded Series (Figure 5d). This component unblocks above $555°C$, producing a sharp boundary between C2 and C1 in thermal demagnetization data where both components are visible. The mean C2 direction is $171/−63°$ ($\kappa = 32$; $N = 74$; $\alpha_{95} = 2.9°$; Figures 6b–6c; consistent with the A magnetization direction of *Xu et al.* [1997]). Xu et al. suggest that the high-temperature magnetization is associated with fine-grained magnetite inclusions in plagioclase. Most of our samples in which C2 was the dominant component have low susceptibilities ($\sim 100 \ \mu SI$) and are plagioclase rich, consistent with Xu et al.'s interpretation. The C1 component may represent a later, possibly thermal, overprint.

3.3. Lightning

[14] Stillwater Complex rocks exposed on the Beartooth Plateau run the risk of acquiring a lightning-induced isothermal remanent magnetization (IRM) during the frequent summer thunderstorms. Lightning-struck samples can be identified

Figure 4. Thermal and alternating field demagnetization of natural remanent magnetization (NRM) illustrating two main types of demagnetization behavior. (a) Vector difference sum (VDS) NRM decay during thermal demagnetization of plagioclase-rich specimen from site pp153. Blue area from 500 to 600°C is enlarged in inset. (b) Decay of VDS remanence in alternating field demagnetization of sister specimen from site pp153. (c) As in Figure 4a, but for orthopyroxenite cm009. (d) As in Figure 4b, but for three cm009 specimens. Note the persistent remanence at high AF values. This is likely gyroremanence: cm009 was not demagnetized using the "Zijderveld-Dunlop" treatment described in section 3. (e–f) Histogram of VDS median destructive temperature (Figure 4e) and field (Figure 4f) for all specimens from pilot study.

using a combination of AF demagnetization and deviations between magnetic and sun compass orientations [*Tauxe et al.*, 2003]. Several plateau specimens in the pilot study produced curved vector endpoint diagrams of the type observed by Tauxe et al. in lightning-struck specimens (Figure 5g). Many of the Stillwater sites with high NRM intensities and low-coercivity components also yielded curved vector endpoint diagrams when thermally demagnetized. The NRM of many of these same specimens (e.g., 4.12×10^{-5} Am^2 for pp013a2 and 4.73×10^{-4} Am^2 for pp018b in Figure 5g) was at least an order of magnitude more intense than that of the rest of the pilot specimens, comparable to typical saturation IRM intensities for the same rock types. In some cases, the strong IRM led to large discrepancies between sun compass orientations and magnetic orientations. Therefore, a combination of factors, high NRM intensity, pilot specimens with low coercivity, and curved thermal demagnetiza-

tion vector endpoint diagrams, were used to identify sites that had been struck by lightning. These sites were excluded from the paleointensity study.

3.4. Remanence Carrier

[15] Thermal and AF data from the pilot study are consistent with a remanence predominantly carried by single-domain (or SD-like) magnetite present as elongate, silicate-hosted particles [*Gee et al.*, 2004; *Selkin et al.*, 2000; *Xu et al.*, 1997]. Hysteresis measurements indicate a high ratio of saturation remanence to saturation magnetization in rocks with the same (C2) high-temperature component [*Selkin et al.*, 2000] and are also consistent with the presence of fine-grained magnetite. Scanning electron microscopic observations of ~300 thin sections from the Stillwater (most from the Middle Banded Series) have revealed essentially no coarse (>5 μm) Fe-Ti oxide grains (except in the massive anorthosites) below the level in Gabbronorite III at

Figure 5

Table 2. Principal Components of Remanence From Pilot Study

Component	Geographic Coordinates	Tilt-Corrected	Anisotropy-Corrected, Tilt-Corrected
C0	323/27 (k = 2.8, N = 52)		
C1	106/−60 ° (κ = 7; N = 177)	175/−32° (κ = 7; N = 177)	175/−34° (κ = 8; N = 96)
C2	064/−48° (κ = 9; N = 156)	167/−60° (κ = 9; N = 156)	171/−63° (κ = 32; N = 74)

which magnetite becomes a cumulate phase [*Meurer and Boudreau*, 1996; *Meurer and Meurer*, 2006]. Concentrations of magnetic oxides in the Stillwater Complex rocks are likely too low and the grain sizes too fine to be noticed. However, hysteresis data indicate that sparse coarse magnetite must be reasonably common throughout the Stillwater Complex (Figure S1 in the auxiliary material) [*Selkin*, 2003].

3.5. Geochronology

[16] Previous geochronologic investigations (Table 1) suggest that the crystallization age of the Stillwater Complex is between about 2.6 and 2.7 Ga. However, the cooling age of the complex, presumably the age of any remaining TRM in the Stillwater, is unclear from these studies. U-Pb zircon and baddeleyite dates provide the most precise interpreted (crystallization) age of the complex, at 2.705 ± 0.004 Ga [*Premo et al.*, 1990]. However, some U-Pb and Pb-Pb dates suggest a younger age (∼2.65 Ga) [*Lambert et al.*, 1985], similar to that of a diabase dike that crosscuts the Stillwater [*Longhi et al.*, 1983].

[17] To better determine the age of the Stillwater's remanence, we carried out step- and single-heating ^{40}Ar-^{39}Ar thermochronology on Stillwater amphibole and biotite separates. The amphibole samples were taken from anorthosite AN-I (see Figure 2) at Picket Pin Mountain. The biotite crystals were collected in the Peridotite Zone, about 1 km from the base of the Stillwater Complex, in the Stillwater Valley. The Ar closure temperature of amphibole (∼550°C) [*Harrison*, 1982] approximates the lowermost unblocking temperatures of the C2 component. Biotite's closure temperature is considerably lower (∼250°C) [*Harrison et al.*, 1985].
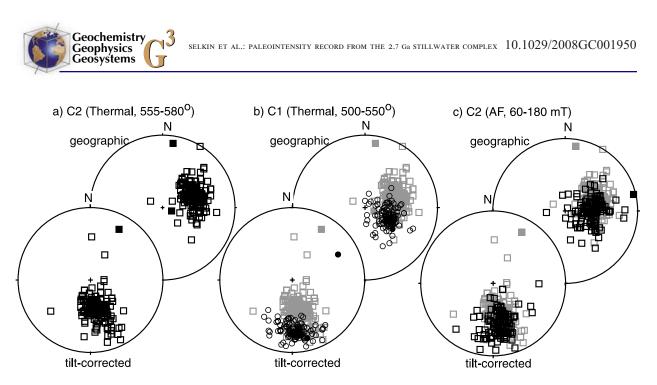
[18] The Stillwater Complex Ar-Ar dates, while poorly constrained, are consistent with an age of the C2 component close to that of the Stillwater's crystallization (see Figure S2 and Table S2 in the auxiliary material and captions for methodology, release spectra, and isotope data). Biotites were characterized by complex release spectra and a wide range of ages: these data are not considered further. However, amphibole Ar-Ar single step laser fusion of seven individual crystals yielded six analytically reliable results and a range of apparent ages between 2.602 ± 0.011 and 2.808 ± 0.009 Ga (mean: 2.701 ± 0.085 Ga). Nine laser step heating experiments on small populations of amphibole grains yielded a single plateau defined by at least 75% of the ^{39}Ar and at least three contiguous steps within 2σ of each other. This plateau (defined by 12 steps) yields an age of 2.744 ± 0.011 Ga. These geochronologic data along with the contact test reported by *Xu et al.* [1997] suggest that the Stillwater Complex has not undergone heating above 550°C since the late Archean.

4. Paleointensity Study

4.1. Methods

[19] We carried out Thellier-type paleointensity determinations on a total of 441 ∼10 cm³ specimens from 188 sites. Of those specimens, the majority either come from sites with a remanence dominated by the C2 component (>50% of the NRM as determined in the pilot study) or have low susceptibility (a characteristic of many of the specimens with a remanence dominated by the C2 component). We also selected some specimens from sites where only a C1 component was iden-

Figure 5. Vector endpoint diagrams for representative Stillwater specimens, showing C0, C1, and C2 components and lightning strikes. Open symbols indicate projections on vertical plane. Filled symbols indicate horizontal plane. (a) Site pp060, showing C0, C1 and C2 components in thermal demagnetization, and C0 and mixed C1/C2 in AF demagnetization. (b–c) Sites pp074 and cl079 showing mainly C1 component; C0 component is recognizable in cl079. (d–e) Sites pp153 and pp055 with only C2 identifiable. (f) Site cm009 with only C1 component identifiable. (g) Specimens likely struck by lightning. All data are shown in geographic coordinates.

Figure 6. Directions of principal components isolated during thermal and AF demagnetization. All plots are equal area projections. Open symbols indicate upper hemisphere. Filled symbols indicate lower hemisphere. Right-hand plots of each pair are in geographic coordinates; left-hand plots are corrected for tilt of igneous layering (304/57°). Data are not corrected for the effects of anisotropy; see Table 2 for anisotropy-corrected mean directions. (a) High-temperature C2 components isolated by thermal demagnetization. Mean direction: 167/−56°. (b) Moderate-high temperature C1 component isolated by thermal demagnetization. Mean direction: 176/−21°. Grey points are C2 directions from Figure 6a. (c) High-coercivity component isolated in AF demagnetization. Mean direction: 171/−42°. Grey points are C2 directions from Figure 6a.

tified in the pilot study. Stratigraphically, sites ranged from the Upper Banded Series to the Bronzitite Zone in the Ultramafic Series.

[20] The modified Thellier experiment [*Coe*, 1967; *Riisager and Riisager*, 2001; *Thellier and Thellier*, 1959; *Yu et al.*, 2004] is the only paleointensity technique that provides for a check for the effects of alteration during the course of the experiment. Thellier-type experiments require stepwise demagnetization (i.e., heating to a temperature T_i less than the Curie temperature, T_C, and cooling in null field, followed by measurement) and remagnetization (heating to T_i and cooling in a known field, followed by a second measurement). In this study, temperature increments in the paleointensity experiments were typically 10°C from 500 to 550°C and 5°C from 550 to 580°C. To check that samples are not altering during the experiment, we have included pTRM checks [*Coe*, 1967], multi-domain pTRM tail checks of *Riisager and Riisager* [2001; see also *Yu and Dunlop*, 2003], and the IZZI technique of *Yu et al.* [2004]. The pTRM checks involve the repetition of earlier in-field heating-cooling steps (heating to a lower temperature and cooling in the same known field, followed by measurement). *Riisager and Riisager* [2001] claim that a second demagnetization step at T_i following

a remagnetization step at T_i will discriminate between single-domain and multidomain magnetic carriers; these steps are the pTRM tail checks, which we carried out on most specimens. Both pTRM and tail checks were typically carried out at every other temperature step. In addition, for most specimens, we followed the IZZI sequence of heating steps [*Yu et al.*, 2004], reversing the order of the double heating at every other temperature step (i.e., demagnetization followed by remagnetization at T_i, then remagnetization followed by demagnetization at T_{i+1}) to detect differences between blocking and unblocking temperature spectra. Following the paleointensity experiment, the anisotropy of anhysteretic remanence (AARM) tensor and TRM acquisition as a function of applied field were determined for each successful paleointensity specimen (discussed in more detail in section 4.3).

4.2. Reliability Criteria

[21] To determine whether paleofield estimates accurately reflect the ancient field at the time when the rocks acquired their TRM, it is necessary (though not sufficient) to examine several indicators of the experiments' reliability. A variety of criteria have been proposed to assess the quality of a paleointensity estimate [see, e.g., *Tauxe*, 2006].
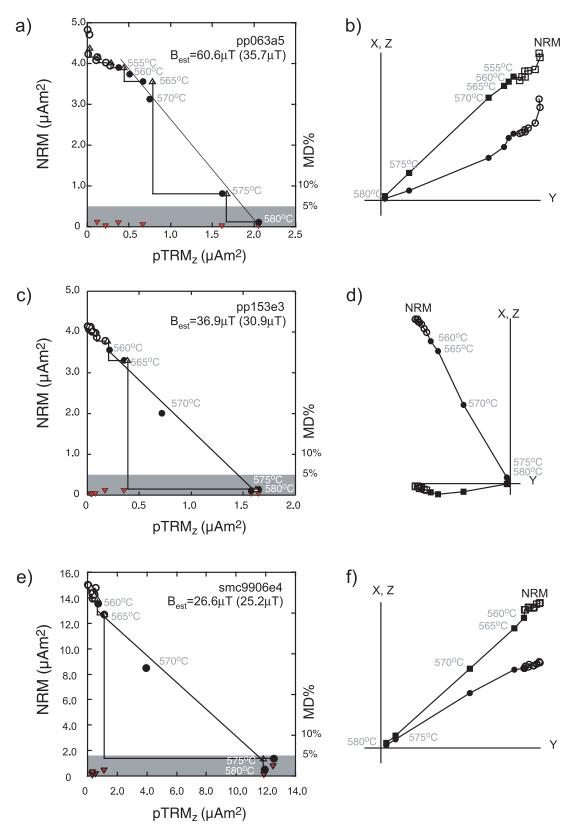
Figure 7

Many of these quality indicators can be illustrated on plots of NRM remaining versus pTRM gained at each temperature step [*Nagata et al.*, 1963] (e.g., Figures 7 and 8). Reliability criteria are necessarily somewhat arbitrary, but we feel that the ones chosen here represent criteria at least as stringent as those applied to paleointensity data from younger rocks (see Figure S3 and Table S3 in the auxiliary material for comparison to *Tauxe* [2006]). In summary, successful paleointensities in the context of this study must have an NRM fraction *f* of 30% or more, a principal component that trends toward the origin ($\alpha < 5°$), pTRM checks that agree closely with the initial pTRMs (DRAT $\leq$ 10%), and pTRM tail checks that agree closely with corresponding zero-field steps (MD% $\leq$ 5%).

[22] Data from sites with only a single otherwise successful specimen must have a well-characterized best fit NRM-pTRM line ($\sigma/|b| \leq 0.1$) and principal component direction (MAD $\leq$ 10°). We believe these criteria to be too stringent to apply to all specimens: for most specimens, the NRM-pTRM data are scattered not because of multidomain behavior, but because the narrow range of unblocking temperatures would require experiments to be carried out with temperature reproducibility beyond that of our ovens in order to achieve $\sigma/|b| \leq 0.1$. Nonetheless, 81% of the otherwise successful paleointensity data from all sites (multispecimen and single-specimen) fulfill the $\sigma/|b|$ and MAD criteria, and all but four of those that do not fulfill the $\sigma/|b|$ criterion have $\sigma/|b| \leq 0.15$.

[23] To confirm the standard assumption that the NRM lost in an experiment is proportional to pTRM gained (or at least that proportionality is a reasonable approximation), we also require that all successful samples pass a TRM saturation criteria. We therefore calculate the percent of TRM saturation (SAT, the TRM gained at 600°C in an applied field equal to the ancient field, normalized by the scale parameter α of the hyperbolic tangent fit $M_{TRM} = \alpha \tanh[\beta \, B_{anc}]$), and require that SAT be less than 80% for all successful paleointensities. A

more detailed explanation of the need for this criterion and of the corresponding correction for nonlinear TRM is found in section 4.3 and in the work of *Selkin et al.* [2007].

[24] We do not apply any site-level criteria as *Tauxe* [2006] does, but we will separate sites according to number of specimens ($N_{spec} \geq 2$) and within-site scatter ($\sigma_B/B_{anc} \leq 15\%$ or $\sigma_B \leq 5\mu T$) in our analysis.

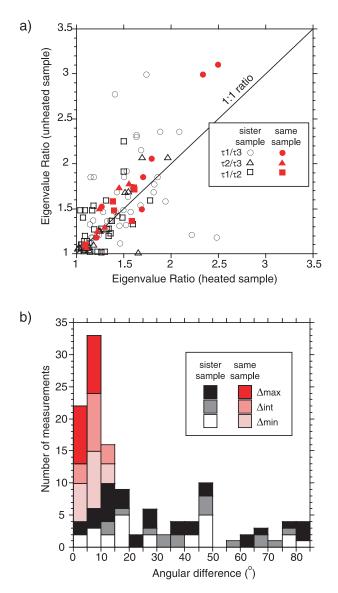## 4.3. Anisotropy, Cooling Rate, and Nonlinear TRM Acquisition

[25] Because many of the specimens chosen for this study have large remanence anisotropies, we applied a correction (following *Selkin et al.* [2000]) to the NRM-pTRM points, the pTRM checks and the MD tail checks based on AARM measurements made (primarily) after the specimens were heated. In some cases, the AARM tensor, especially if measured after heating, may not be appropriate to correct for TRM anisotropy. The magnitude of AARM is not identical to that of TRM anisotropy, and the AARM tensor may change during the course of a heating in a paleointensity experiment. To demonstrate that the AARM tensor has not changed during heating, we compared the eigenvalues (Figure 9a) and eigenvectors (Figure 9b) of AARM tensors from heated specimens to their unheated counterparts. This was done for two sets of specimens. At 24 sites, we were able to compare the AARM tensor, measured after heating, from a successful paleointensity specimen to the tensor from a nearby ("sister") unheated specimen. In addition, at 18 other sites that yielded acceptable paleointensity data, we measured AARM tensors on a nonpaleointensity specimen before and after a single-step heating to 600°C. Most of the AARM tensors are similar before and after heating, falling on or near the 1:1 line on Figure 9a and below 10° on Figure 9b. However, several samples have tensors that are different before and after heating. Most of these samples are from sites that have significant within-site lithologic variability (e.g.,

Figure 7. (left) NRM-pTRM (Arai) plots and (right) vector endpoint diagrams for successful paleointensity determinations. In NRM-pTRM plots, circles represent NRM-pTRM pairs; open upward pointing triangles represent pTRM checks. Vector endpoint diagrams are in sample coordinates. Squares represent projection of NRM vector onto horizontal plane. Circles represent projection onto vertical plane. Labeled temperature steps (on both plots) and filled symbols represent data used to determine best fit line [*York*, 1967, 1968]. B_{est} is the uncorrected estimates of ancient field based on data marked as filled symbols. Open triangles represent pTRM checks. Downward pointing triangles represent MD tail checks. Gray region represents 5% cutoff for MD tail checks. Parentheses represent estimates of ancient field adjusted to compensate for nonlinear TRM acquisition, anisotropy, and slow cooling in nature. (a−b) Specimen pp063a5. (c−d) Specimen pp153e3. (e−f) Specimen smc9906e4. All specimens pass all reliability criteria.

Figure 8. (left) NRM-pTRM (Arai) plots and (right) vector endpoint diagrams for unsuccessful paleointensity determinations and for a C1 paleointensity. Symbols as in Figure 8. (a–b) Curved NRM-pTRM plot and high values of MD% characteristic of multidomain ferromagnetic grains. (c–d) pTRM checks do not agree with NRM-pTRM points, indicating that the sample is altering during the Thellier experiment. (e–f) Low unblocking temperatures associated with the C1 component. The latter is likely a thermal overprint.
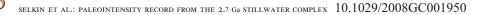
Figure 9. Comparison of AARM tensors before and after heating. "Sister samples" refers to the comparison of pairs of tensors from adjacent specimens, one of which yielded paleointensity results that passed the selection criteria. The AARM of the paleointensity specimen was measured after heating. "Same samples" refers to specimens taken from sites that yielded at least one successful paleointensity. AARM was measured on (nonpaleointensity) specimens from several such sites both before and after a single heating to 600°C. (a) Comparison of heated and unheated AARM tensor eigenvalues. Line ("1:1 ratio") indicates no change during heating. (b) Angular difference between eigenvectors of heated and unheated AARM tensors. For both Figures 9a and 9b, only results that passed appropriate F tests [*Hext*, 1963] are shown.

sites pp147–148, which contain lenses of anorthosite and 2–3 cm orthopyroxene oikocrysts, and site pp161, which contains coarse orthopyroxene). Comparing nearby samples of such heterogeneous rocks may be misleading, because adjacent samples may contain minerals with significantly different magnetic properties. Pairs of AARM tensors from the same specimens are more similar than pairs of tensors from sister specimens. Based on this comparison, we conclude (similarly to *Selkin et al.* [2000]) that the AARM correction at least partially counteracts the effects of TRM anisotropy in paleointensity experiments where specimens are not altered during heating (i.e., specimens that pass their pTRM checks).

[26] The slow cooling of plutons like the Stillwater Complex can also affect paleointensity estimates: slowly cooled rocks acquire a more intense TRM than do rocks cooled quickly in laboratory ovens [*Halgedahl et al.*, 1980; *Selkin et al.*, 2000]. To estimate the difference between the natural and laboratory cooling rates, we modeled the cooling of the Stillwater both using a 1-D finite difference conductive cooling model and using an analytic half-space model (Figure S4 and Tables S4 and S5 in the auxiliary material; initial and boundary conditions consistent with *Labotka and Kath* [2001] and approximately consistent with *Thomson* [2008]). Although the Archean geotherm is not well known, the temperature gradient used in the model did not substantially affect the cooling rate. In contrast, hydrothermal convection at the top of the intrusion may significantly increase the cooling rate [*Coogan et al.*, 2002]. Several runs of the models with different initial temperature conditions yielded similar results (e.g., Figure S4 and Table S5 in the auxiliary material): sites at depths of 0.5–5.5 km from the top of the intrusion take ~50–200 ka to cool through the range of blocking temperatures associated with the C2 component (550–580°C). Convective cooling may increase cooling rates by nearly an order of magnitude [*Coogan et al.*, 2002]. Sites in the Stillwater complex may therefore have taken as little as 20 ka to cool. Sites at the bottom of the complex cool through their minimum blocking temperature about 1 Ma later than do sites near the top of the pluton.

[27] The difference between the predicted cooling rate of the Stillwater Complex Banded Series rocks (a few degrees per 10 ka) and the laboratory cooling rate (a few degrees per second) would cause a Thellier-type paleointensity experiment to

overestimate the ancient field by about 40% [*Bowles et al.*, 2005; *Halgedahl et al.*, 1980; *Selkin et al.*, 2000]. The difference between the cooling rate correction used here and that used by *Selkin et al.* [2000] (45%) is the faster natural cooling rate used here. The cooling rate correction assumes that the paleointensity estimate is based on remanence carried by noninteracting single-domain magnetic particles. If the particles do not acquire a TRM like single-domain particles, the cooling rate correction used here may mean that our paleofield estimates represent a lower bound on the actual ancient field intensity. Furthermore, because the cooling rate estimated here does not take convective cooling into account, the cooling rates may be much faster than estimated. For this reason as well, the data adjusted for cooling rate may be lower than the actual paleofield.

[28] A previous study of TRM acquisition indicated that rocks with elongate magnetic particles acquire TRM as a nonlinear function of applied field, even in applied fields as weak as 10s of μT [*Selkin et al.*, 2007]. TRM acquisition data indicate that this is the case for many of the specimens in this study. Therefore, a correction for nonlinear TRM acquisition (outlined in the work of *Selkin et al.* [2007]) has been applied to the paleointensity estimates discussed here.

[29] All of the results discussed in the following sections represent paleointensities corrected for the effects of anisotropy, cooling rate, and nonlinear TRM acquisition. However, in the auxiliary material, we also tabulate uncorrected results. The effects of each correction are also summarized as histograms in Figure S5 in the auxiliary material.

5. Results

[30] We chose 441 core specimens from 188 sites for paleointensity experiments. Of these, 414 have an appreciable C2 component, in that over 30% of their original NRM remained after heating to 555°C. Principal component directions from oriented specimens (mean direction: 169/−61° in tilt-corrected coordinates) are similar to the mean C2 direction from thermally demagnetized specimens (171/−63°). A total of 114 specimens from 53 sites passed the reliability criteria listed above (Table 3; Figure S3 and Table S3 in the auxiliary material). Of these sites, 17 were represented by a reliable paleointensity from only one specimen. Specimen- and site-level paleointensity data from this study are available in Tables S6 and S7 in the auxiliary

material. Raw paleointensity data are also available in the MagIC database.

[31] In all but a few of the multiple-specimen sites, the estimated paleointensities agree to within a few μT. The average within-site standard deviation (σ_B) is 3.9 μT (average σ_B/B_{anc}: 12.5%). Seven sites have standard deviations higher than the limits set by *Tauxe* [2006] ($\sigma_B/B_{anc} < 0.15$ or $\sigma_B < 5\mu$T). We label these "high-scatter" sites and treat them separately.

[32] Although the 188 sites chosen for paleointensity experiments spanned a stratigraphic interval from the Upper Banded Series to the Bronzitite Zone in the Ultramafic Series, the reliable paleointensities were mainly from plagioclase-rich rocks of the Upper Banded Series (Figure 10). No reliable paleointensities were recovered from stratigraphic levels below Olivine Bearing Zone III in the Middle Banded Series. Most of the successful paleointensity results came from Stillwater Mining Company cores from the East Boulder mine adit. We attribute this success mostly to the large number of specimens from plagioclase-rich intervals obtained from the SMC cores and to the freshness of the rocks in the cores.

[33] The mean of all site mean paleointensities that pass the reliability criteria is 30.6 ± 8.8 μT (31.4 ± 8.8 μT including high-scatter sites). As noted above, these values are corrected for the effects of remanence anisotropy, cooling rate, and nonlinear TRM acquisition. Reliable paleointensities range from 11.1 to 59.8 μT.

[34] To compare results from the Stillwater with paleointensities from elsewhere, we report paleointensities in terms of their virtual dipole moment (VDM), the equivalent geocentric dipole moment required to produce the observed paleointensity. VDMs of individual sites range between 1.84 × 10^{22} and 9.87 × 10^{22} Am^2. The mean of site mean VDM values is 5.05 ± 1.46 × 10^{22} Am^2 (5.18 ± 1.45 × 10^{22} Am^2 including high-scatter sites).

6. Discussion
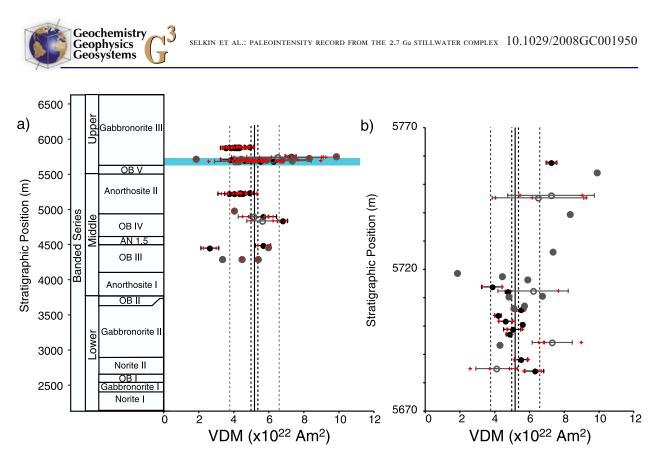
6.1. Origin of Remanence

[35] In the rocks from the Stillwater Complex used in this study, magnetite is inferred to exist primarily as oriented particles included in silicates rather than as discrete grains [*Xu et al.*, 1997]. To demonstrate that the remanence in Stillwater rocks is carried by silicate-hosted rather than discrete magnetite grains, we separated plagioclase, clino-

Table 3. Successful Site Mean Paleointensities From Stillwater Complex Rocks[a]

Site	N	B_{est} (μT)	B_{anc} (μT)	B_{anc}* (μT)	B_{anc}** (μT)
pp043	2	20.37 ± 3.40	20.39 ± 3.53	22.38 ± 4.41	15.98 ± 3.15
pp055	2	48.04 ± 3.27	49.03 ± 3.78	48.33 ± 3.65	34.52 ± 2.61
pp056	1	62.81	66.78	57.20	40.85
pp057	2	38.69 ± 2.33	44.21 ± 2.63	40.23 ± 1.13	28.74 ± 0.80
pp058	2	50.89 ± 16.71	59.15 ± 28.40	52.68±17.34	37.63 ± 12.39
pp060	3	32.39 ± 4.48	32.44 ± 4.48	32.56 ± 4.90	23.26 ± 3.50
pp063	1	60.59	62.89	50.02	35.73
pp065	1	32.72	33.15	37.70	26.93
pp068	1	10.26	10.26	15.57	11.12
pp082	1	50.52	50.89	62.19	44.42
pp100	1	60.47	76.08	70.56	50.40
pp110	3	49.75 ± 12.55	58.56 ± 23.24	55.07 ± 22.19	39.34 ± 15.85
pp120	2	49.07 ± 5.81	52.33 ± 8.08	61.48 ± 21.29	43.92 ± 15.21
pp147	1	66.46	69.83	83.73	59.80
pp148	2	54.91 ± 0.62	64.35 ± 0.62	61.65 ± 2.60	44.04 ± 1.86
pp149	1	39.66	45.49	40.68	29.06
pp152	1	36.60	48.38	48.28	34.49
pp153	1	36.85	44.69	43.25	30.89
pp161	1	56.97	67.10	61.43	43.88
pp169	1	29.03	35.35	34.33	24.52
smc9902a	3	41.98 ± 0.99	44.19 ± 1.74	41.46 ± 2.20	29.62 ± 1.57
smc9902b	4	36.43 ± 3.64	37.30 ± 3.98	36.46 ± 3.26	26.04 ± 2.33
smc9902c	4	37.59 ± 2.82	38.63 ± 3.10	34.49 ± 2.85	24.64 ± 2.04
smc9902e	3	34.88 ± 3.01	35.94 ± 3.73	35.32 ± 4.76	25.23 ± 3.40
smc9902f	3	38.89 ± 5.11	40.30 ± 5.56	36.75 ± 5.61	26.25 ± 4.01
smc9902g	3	37.93 ± 4.44	39.16 ± 4.81	34.12 ± 4.89	24.37 ± 3.49
smc9902h	2	34.71 ± 2.47	35.44 ± 2.14	30.04 ± 1.69	21.46 ± 1.21
smc9902j	3	36.84 ± 5.03	37.67 ± 5.25	32.63 ± 5.10	23.31 ± 3.64
smc9903a	3	35.74 ± 2.93	38.90 ± 3.59	46.86 ± 2.03	33.47 ± 1.45
smc9903c	3	32.58 ± 3.37	33.81 ± 3.72	35.53 ± 1.60	25.38 ± 1.14
smc9903d	3	35.90 ± 2.74	38.21 ± 2.81	39.23 ± 3.44	28.02 ± 2.45
smc9903e	2	39.85 ± 0.16	44.34 ± 0.78	47.44 ± 0.76	33.88 ± 0.54
smc9903f	3	38.24 ± 4.22	41.10 ± 4.93	42.60 ± 4.17	30.43 ± 2.98
smc9903g	3	35.53 ± 2.36	37.98 ± 2.27	40.96 ± 1.34	29.26 ± 0.96
smc9903i	4	40.13 ± 4.47	46.84 ± 7.71	62.02 ± 9.67	44.30 ± 6.91
smc9903j	1	39.86	42.28	36.31	25.93
smc9903l	3	32.42 ± 2.73	35.45 ± 2.65	46.83 ± 3.24	33.45 ± 2.31
smc9903m	4	32.93 ± 5.01	34.82 ± 6.09	34.79 ± 10.18	24.85 ± 7.27
smc9903n	3	46.96 ± 1.83	53.98 ± 2.51	53.35 ± 4.55	38.11 ± 3.25
smc9906a	2	32.02 ± 0.13	36.98 ± 1.32	41.53 ± 2.07	29.66 ± 1.48
smc9906c	2	26.27 ± 1.20	31.17 ± 1.89	37.01 ± 0.85	26.43 ± 0.61
smc9906d	3	28.76 ± 1.65	33.08 ± 3.03	38.20 ± 6.99	27.29 ± 4.99
smc9906e	2	24.63 ± 2.82	26.51 ± 1.44	31.63 ± 5.22	22.59 ± 3.73
smc9906f	2	27.91 ± 2.50	31.68 ± 1.26	34.29 ± 4.56	24.49 ± 3.25
smc9906g	3	31.60 ± 0.79	35.39 ± 2.40	36.83 ± 3.23	26.31 ± 2.31
smc9910c	3	43.48 ± 5.00	46.32 ± 5.73	48.33 ± 6.45	34.52 ± 4.61
smc9910d	2	38.92 ± 5.37	41.18 ± 6.38	43.62 ± 7.52	31.15 ± 5.37
smc9914a	2	40.34 ± 3.13	48.00 ± 7.73	47.85 ± 7.37	34.18 ± 5.27
smc9914b	2	40.78 ± 0.41	48.83 ± 2.34	57.70 ± 2.29	41.21 ± 1.63
smc9915b	1	42.53	52.28	50.75	36.25
smc9916f	1	23.66	23.12	28.34	20.24
smc9916i	1	29.33	32.51	37.97	27.12
smc9916h	1	32.95	38.55	45.85	32.75

[a] All paleointensities pass criteria listed in text (see also Figure S3 and Table S3 in the auxiliary material). N is number of specimens. B_{est} is estimated paleointensity, uncorrected. B_{anc} is adjusted to account for nonlinear TRM acquisition. B_{anc}* is adjusted to account for nonlinear TRM acquisition and effects of TRM anisotropy. B_{anc}** is adjusted to account for nonlinear TRM acquisition, anisotropy, and slow cooling. Sites in italics pass σ_B/B_{anc} criterion. Specimen-level data tabulated in Figure S4 and Table S5 in the auxiliary material.

Figure 10. (a) Plot of paleointensity (expressed as virtual dipole moment, VDM) versus stratigraphy for specimens that pass reliability criteria. VDM values have been compensated for the effects of anisotropy, cooling rate, and the nonlinear relationship between TRM and applied field. Red crosses indicate individual specimens. Black filled dots with error bars indicate sites with multiple specimens and low standard deviation (σ < 15% of the mean or σ < 5 μT). Open circles with error bars indicate sites with multiple specimens and high standard deviation. Gray circles indicate single-specimen sites. Stratigraphic column shown for reference. Black vertical line indicates mean paleointensity. Black dotted line indicates standard error about the mean. Gray dotted line: standard deviation (1σ). (b) Expansion of blue area in Figure 10a. Specimen- and site-level data available in Tables S6 and S7 in the auxiliary material.

pyroxene, and orthopyroxene crystals from five rocks from the Middle and Upper Banded Series and imparted an ARM (Table 4). Whole rock samples were also given an ARM (in several different directions to account for anisotropy). In every case, the mean ARM of the mineral phases, weighted by modal proportion, can completely account for the bulk sample ARM when the variability of the single-crystal ARMs are considered. Many of the single crystal separates have a strong remanence anisotropy parallel to the preferred orientation of silicate crystals, which, along with whole-rock anisotropy and crystallographic data [Gee et al., 2004] suggests that the precipitation of the oxide grains is crystallographically controlled.

[36] Although the remanence is carried by silicate-hosted magnetite, the origin of these oxides is uncertain, and their temperature of formation is not easy to determine. In pyroxenes, optimal phase boundary calculations indicate that magnetite precipitates in two crystallographically controlled directions [Feinberg et al., 2004; Feinberg et al.,

2005; Fleet et al., 1980; Renne et al., 2002]. A study by Feinberg et al. [2004] used the optimal phase boundary technique to determine that magnetite in clinopyroxene from the Messum Complex (Namibia) precipitated at temperatures above 800°C. Other studies have obtained significantly lower temperatures using the same geothermometer (e.g., 540 ± 25° [Bogue et al., 1995]; 600° [Fleet et al., 1980]). Simply from the temperature of formation, it appears that clinopyroxene-hosted magnetite may form either at temperatures above or slightly below the Curie point of pure magnetite (580°C); if the formation temperature is below the Curie point then the remanence need not be a simple thermoremanence.

[37] Plagioclase-oxide exsolution is poorly studied when compared to pyroxene [see Feinberg et al., 2005], and the mechanism by which the oxides form is correspondingly unclear. As opposed to pyroxene, there is no geothermometer for the formation of magnetite in plagioclase. However, a qualitative argument for its high-temperature origin

can be made based on the likely slow diffusion of Fe^{3+} at subsolidus ($\sim900°C$) temperatures. Diffusion rates of trivalent ions are slower than divalent ions (which in turn diffuse more slowly than monovalent ions) in plagioclase [*Cherniak*, 2002]. By analogy with dry diffusion rates of trivalent rare earth elements in labradorite [*Cherniak*, 2002], we estimate that diffusion of Fe^{3+} over 1 μm requires temperatures of $\sim800°C$ for time scales of $\sim10^4$ years (a likely upper limit for the time the Stillwater spent at this temperature based on our thermal modeling results). Although diffusion of Fe^{2+} in plagioclase will be significantly faster, diffusion of Fe^{3+} will likely be the limiting factor and may be even more sluggish if a coupled diffusion mechanism is required. For example, the dry CaAl–NaSi diffusion rates in plagioclase [*Grove et al.*, 1984] suggest micron-scale diffusion for the same 10^4 year timescale would require temperatures of 970°C. If correct, this reasoning suggests that plagioclase-hosted magnetite likely forms at temperatures above the Curie temperature of magnetite and the remanence should be a thermoremanence. However, both Fe^{2+} and Fe^{3+} may be incorporated into the plagioclase structure, via simple or coupled substitutions [e.g., *Wilke and Behrens*, 1999], and the exact mechanism and temperature of formation of plagioclase-hosted magnetite remains uncertain.

[38] Recent atomic force microscopy and TEM observations indicate that magnetite-ulvöspinel intergrowths occur in some, but not all, plagioclase- and pyroxene-hosted titanomagnetite [*Feinberg et al.*, 2005, 2006]. Where such intraoxide exsolution is absent the magnetization is thermoremanent, but the miscibility gap responsible for magnetite-ulvöspinel intergrowths is below 600°C (and exsolution may be facilitated by magnetic ordering) and thus the magnetization of grains with intraoxide exsolution should be a thermochemical remanence (TCRM) [*Feinberg et al.*, 2005]. Rocks with a TCRM may not faithfully record paleointensity (*Smirnov and Tarduno* [2005]; however, see also *Draeger et al.* [2006]). It is not known whether the silicate-hosted inclusions in the Stillwater rocks have intraoxide exsolution. Intraoxide exsolution is expected to form a low-Ti, but not Ti-free, titanomagnetite. The observation of the Verwey transition in Stillwater Complex anorthosite specimen M428 by *Kletetschka et al.* [2006] along with Curie temperature data [*Selkin et al.*, 2000; *Selkin*, 2003] support the interpretation that little, if any, Ti is present in the plagioclase-hosted oxides. We tentatively suggest that the plagioclase-hosted

magnetite in the Stillwater, likely carries a thermoremanence (the associated C2 magnetization component).

[39] If the high-stability C2 remanence component is a TRM, or even a high-temperature TCRM, it was likely acquired during the late Archean. The narrow range of high unblocking temperatures of the C2 component suggest that it was acquired at temperatures above 550°C (though prolonged exposure to lower temperatures cannot be ruled out [*Pullaiah et al.*, 1975]). Ar-Ar data reported here and a contact test [*Xu et al.*, 1997] indicate that the Stillwater Complex has not been reheated above the closure temperature of the K-Ar system in hornblende ($\sim T_c$ of magnetite) since the latest Archean.

[40] Nonetheless, the lower-stability C1 magnetization component was likely acquired after the C2 component, indicating some later reheating or grain growth. The association between the C1 remanence component and pyroxene-rich rocks suggests that the C1 component may be carried by magnetite in pyroxene. If the C1 component is a TCRM acquired during exsolution of oxide particles from pyroxene, it should be carried by particles with a range of grain sizes and thus a range of blocking temperatures. The lack of overlap between the blocking temperature ranges of the C1 and C2 components, however, suggests that the C1 component is thermal in origin. The $\sim30°$ separation between directions of the C1 and C2 components is most plausibly explained by a significant gap in time between the acquisition of the C2 component and overprinting by the C1 magnetization.

6.2. Comparison of Stillwater Complex Record With Other Published Paleointensities

[41] Previous studies, based mainly on the hypothesis of *Stevenson et al.* [1983], have posited a link between the nucleation and growth of the inner core and an increase in the Earth's dipole moment [see also *Hale*, 1987; *Tarduno et al.*, 2006]. Comparing the Stillwater Complex data reported here to other paleointensity measurements across the Archean-Proterozoic boundary (Figure 11; Table S8 and Text S1 in the auxiliary material), no steady increase in the Earth's dipole moment over time is evident from the data. Indeed, if one considers only the data obtained using techniques that allow consistency checks during a paleointensity experiment (modified Thellier with pTRM checks, microwave Thellier analog, and single-crystal laser

Table 4. Single-Crystal and Whole-Rock Anhysteretic Remanent Magnetization Measurements[a]

Site	Clinopyroxene ARM (Am²/kg)	N	Mode %	Orthopyroxene ARM (Am²/kg)	N	Mode %	Plagioclase ARM (Am²/kg)	N	Mode %	Whole Rock Predicted (Am²/kg)	Whole Rock Measured (Am²/kg)	N
cm009			0%	$2.89 \times 10^{-05} \pm 2.69 \times 10^{-05}$	43	100%			0%	2.89×10^{-05}	$2.23 \times 10^{-06} \pm 2.33 \times 10^{-05}$	3
pp002			0%			0%	$2.53 \times 10^{-04} \pm 2.12 \times 10^{-04}$	45	100%	2.53×10^{-04}	1.22×10^{-04}	1
pp034	$2.86 \times 10^{-04} \pm 5.91 \times 10^{-06}$	34	10%	$6.35 \times 10^{-05} \pm 6.66 \times 10^{-05}$	45	10%	$5.70 \times 10^{-05} \pm 4.35 \times 10^{-07}$	43	80%	8.06×10^{-05}	$7.74 \times 10^{-05} \pm 1.77 \times 10^{-05}$	5
pp046	$7.15 \times 10^{-05} \pm 2.42 \times 10^{-04}$	46	10%	$1.69 \times 10^{-04} \pm 1.21 \times 10^{-04}$	39	10%	$1.27 \times 10^{-04} \pm 7.41 \times 10^{-05}$	49	80%	1.26×10^{-04}	$8.19 \times 10^{-05} \pm 2.62 \times 10^{-06}$	6
pp074	$7.45 \times 10^{-04} \pm 1.17 \times 10^{-03}$	28	10%	$6.91 \times 10^{-05} \pm 2.46 \times 10^{-04}$	46	15%	$7.23 \times 10^{-05} \pm 5.05 \times 10^{-05}$	47	75%	1.39×10^{-04}	$1.72 \times 10^{-04} \pm 4.75 \times 10^{-05}$	6
pp067			0%	$2.10 \times 10^{-03} \pm 1.09 \times 10^{-04}$	39	10%	$1.53 \times 10^{-04} \pm 4.11 \times 10^{-06}$	47	90%	3.47×10^{-04}	$1.45 \times 10^{-04} \pm 4.44 \times 10^{-05}$	5

[a] In all experiments, anhysteretic remanent magnetization (ARM) imparted using 180 mT peak alternating field with 0.1 mT bias field. Predicted whole-rock ARM values are averages based on single-crystal measurements, weighted by mode percent.
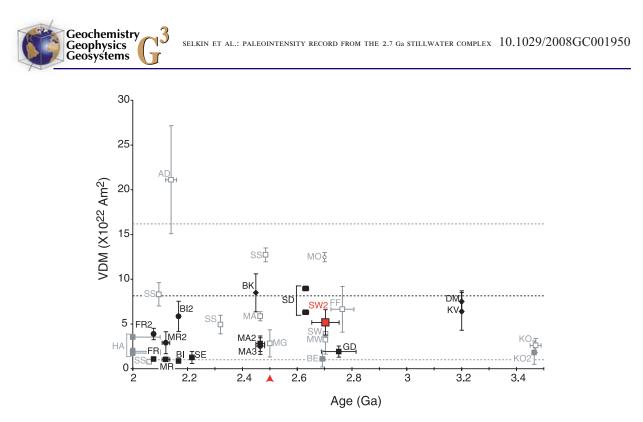
Thellier analog), and avoids paleointensities from rocks with clear evidence of metamorphism, Earth's dipole moment appears to have varied almost as widely across the Archean-Proterozoic boundary as it has in the Phanerozoic [*Tauxe*, 2006]. The average VDM reported here is between the VDM reported by *Morimoto et al.* [1997] for a 2.8 Ga dolerite dike in west Greenland, and two VDMs reported by *Yoshihara and Hamano* [2000] for ∼2.6 Ga dikes from the Slave Craton. However, it would be misleading to interpret these three data as constituting a trend: the ∼100 Ma gaps between each of these three data points are comparable to the entire 160 Ma time span of a recent analysis of the Phanerozoic field [*Tauxe*, 2006]. Therefore, the sparseness of the Archean-Proterozoic data would make it difficult to identify a trend even if one did exist.

6.3. Statistical Properties

[42] The sites in this study are likely to sample the field during a substantial time interval and are sufficiently numerous to provide some information on the statistical variations of the Archean field. The distribution of Stillwater Complex VDMs is statistically indistinguishable from a lognormal distribution (Figure 12a; $\mu = 50.32$; $\sigma = 0.93$; Lilliefors test: maximum difference $d = 0.0990$, critical value $d_{crit}(0.05) = 0.1211$, $p = 0.2123$) a distribution proposed for Phanerozoic paleointensity data [e.g., *Tanaka et al.*, 1995]. However, the distribution of VDMs is much more tightly concentrated around the mean than is the distribution of Phanerozoic VDM estimates [see, e.g., *Tauxe*, 2006] (Figure 12b), as might be expected given the inherent averaging that would be imparted by slow cooling.

[43] Comparison with results from the Tudor Gabbro, a ∼1.1 Ga intrusion in southern Ontario [*Yu and Dunlop*, 2001] with a substantial number of sites, further supports the idea that the narrow distribution of intensities from the Stillwater is the result of slow cooling. *Yu and Dunlop* [2001] obtained paleointensities from 45 specimens from nine sites using a procedure similar to the one we employed. The Tudor Gabbro may have cooled through the relevant blocking temperature range in as little as a few ka [*Yu and Dunlop*, 2001] or as long as a few tens of thousands of years (based on our calculations using the same 1-D conductive cooling models as for the Stillwater Complex). Although the Stillwater Complex distribution has a high-VDM tail not observed in the Tudor Gabbro data (Figure 12c),
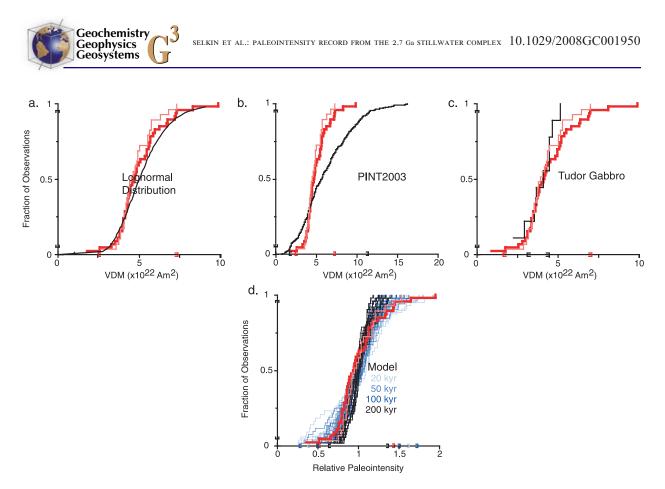
Figure 11. Paleointensities obtained from rocks formed prior to 2.0 Ga. Two-letter codes and references are explained in Table S8 and Text S1 in the auxiliary material. Error bars are 1σ in both age and VDM. Red arrow indicates Archean-Proterozoic boundary (2.5 Ga). Red symbol indicates this study. Black squares indicate whole-rock Thellier-type experiments with pTRM checks. Black diamonds indicate single-crystal Thellier-type experiments with pTRM checks. Black circles indicate microwave Thellier-analog experiments. Gray filled symbols indicate whole-rock Thellier-type experiments (with pTRM checks) on chemically altered rocks. Gray open squares indicate Thellier-type experiments without pTRM checks. Gray circle indicates non-Thellier experiment. Black dotted line indicates Earth's present dipole moment. Gray dotted lines indicate approximate range of VADM from Phanerozoic rocks [*Tauxe*, 2006].

the two distributions are statistically indistinguishable (Kolmogorov-Smirnov test [*Rice*, 1995] when the 24 high-scatter or single-specimen sites are not included: maximum difference $d = 0.2069$, critical value $d_{crit}(0.05) \approx 0.5$, $p = 0.8947$; including high-scatter sites: $d = 0.3462$, $d_{crit}(0.05) = 0.4903$, $p = 0.2552$).

[44] To further illustrate the possible effect of slow cooling, we can simulate paleointensity records that we would expect to obtain from slowly cooled intrusive rocks that sample a length of time similar to the Stillwater Complex record. We use a moving average across a set of "known" paleointensity variations to simulate the averaging due to slow cooling [*Selkin*, 2003]. We use the 11-Ma-long Oligocene relative paleointensity record from Deep Sea Drilling Program Hole 522 [*Hartl and Tauxe*, 1997] as the underlying relative paleointensity variations in our model. In this model, the degree of smoothing is related to the time each site takes to cool through the 580–550°C range of blocking temperatures (Δt_{site}). The time interval over which the entire pluton cools determines the time span of the entire record ($t_{total} = 1$ Ma), throughout which

the collection of sites ($n_{pts} = 52$) are spaced. Because the DSDP 522 record is much longer than t_{total}, we ran the model using several 1-Ma segments of the data set.

[45] The smoothing imparted by temporal averaging of the sedimentary relative intensity record (results of ten 1 million year time intervals shown by black lines in Figure 12d) is similar to the distribution of normalized Stillwater Complex paleointensities. For cooling times (Δt_{site}) of 20–200 ka that represent plausible bounds (with the lower value reflecting hydrothermal cooling and the upper value simple conduction) for the Stillwater Complex, we find that the Stillwater paleointensity distribution is within the range of modeled distributions. It therefore appears that plausible values of slow cooling (1.5 to 0.15°C/ka) could reduce the variance in paleointensity from that observed in the DSDP 522 record (or that observed in the database of absolute paleointensities from the Phanerozoic) to that observed in the Stillwater Complex data set. Overall, we find no compelling evidence that geomagnetic field

Figure 12. Cumulative distribution functions (CDFs) of Stillwater data (anisotropy, cooling-rate, and nonlinear TRM acquisition corrected) compared to models and paleointensity data sets. In all plots, CDFs of Stillwater Complex VDMs that pass reliability criteria are drawn in red (bold indicates all sites; thin indicates multiple-specimen, low-scatter sites). Black brackets on vertical axis indicate 5th and 95th percentiles. Red brackets on horizontal axis enclose 95% of the range of the Stillwater data. Black brackets indicate 95% range of comparison data. (a) Comparison with lognormal distribution (parameters estimated using all reliable Stillwater Complex sites; $\mu = 50.32$; $\sigma = 0.93$). Black solid line indicates lognormal distribution. (b) Comparison between Stillwater Complex and published Thellier paleointensity data set [*Tauxe*, 2006]. Note change in horizontal scale from Figure 12a. (c) Comparison between Stillwater Complex and Tudor Gabbro site mean VDMs [*Yu and Dunlop*, 2001]. (d) Comparison between normalized Stillwater Complex and model based on Oligocene relative paleointensity record [*Hartl and Tauxe*, 1997]. Note change in horizontal scale. Blue and black lines indicate model paleointensity distributions produced using 20–200 ka sliding windows (light blue indicates 20 ka; medium blue indicates 50 ka; dark blue indicates 100 ka; black indicates 200 ka) over 1 Ma.

behavior in the Archean differed significantly from that in more recent times.

7. Conclusions

[46] Although the results from the Stillwater should be interpreted with the same caution as other very ancient paleointensities, the 114 successful paleointensities reported here suggest that the mean intensity and variability of the Archean geomagnetic field was similar to that of more recent times. The Stillwater Complex paleointensities, when combined with other paleointensity data from the Archean and early Proterozoic, do not indicate any long-term trends in Earth's average dipole moment, in contrast to the conclusions

of *Hale* [1987; see also *Stevenson et al.*, 1983]. *Hale* [1987] suggested that a distinct increase in the Earth's dipole moment close to the Archean-Proterozoic boundary was a result of the nucleation of the inner core and the initiation of the geodynamo. Our data are more consistent with recent studies [e.g., *Tarduno et al.*, 2007], which suggest that the Archean geodynamo was already capable of generating a dipole-dominated field. Nonetheless, many of the details of early geodynamo activity remain poorly constrained. The future of Archean paleomagnetic studies will require the integration of paleointensity, magnetostratigraphic, and directional records of paleosecular variation to provide a synoptic view of the early geodynamo.

[47] A key component of future Archean paleomagnetic studies must be a focus on obtaining reliable measurements of the ancient field. This study highlights the need not only for high temporal resolution paleomagnetic studies of Archean rocks, but for studies of high technical quality. Specifically, paleointensity estimates, obtained using methods with internal consistency checks and materials likely to carry an Archean TRM, are necessary to validate theoretical studies of the Archean geodynamo. Most of the Archean and early Proterozoic rocks from which paleointensities have been measured are plutonic or hypabyssal rocks as likely, if not more likely, to carry a CRM or TCRM than a TRM. Improvements in distinguishing how remanence is acquired in these rock types [e.g., *Feinberg et al.*, 2005, 2006; *Smirnov and Tarduno*, 2005], along with improved experimental techniques to detect and minimize problems specific to slowly cooled rocks will improve our confidence in the Archean paleointensity record.

Acknowledgments

References

Bergh, H. W. (1970), Paleomagnetism of the Stillwater complex, Montana, in *Paleogeophysics*, edited by S. K. Runcorn, pp. 143–158, Academic, London.

Biggin, A. J., G. H. M. A. Strik, and C. G. Langereis (2008), Evidence for a very-long-term trend in geomagnetic secular vatiation, *Nature Geosci.*, *1*, 395–398, doi:10.1038/ngeo181.

Bogue, S. W., C. S. Grommé, and J. W. Hillhouse (1995), Paleomagnetism, magnetic anisotropy, and Mid-Cretaceous paleolatitude of the Duke Island (Alaska) Ultramafic Complex, *Tectonics*, *14*, 1133–1152, doi:10.1029/95TC01579.

Bowles, J., J. S. Gee, D. V. Kent, E. Bergmanis, and J. Sinton (2005), Cooling rate effects on paleointensity estimates in submarine basaltic glass and implications for dating young flows, *Geochem. Geophys. Geosyst.*, *6*, Q07002, doi:10.1029/2004GC000900.

Buffett, B. A. (2002), Estimates of heat flow in the deep mantle based on the power requirements for the geodynamo, *Geophys. Res. Lett.*, *29*(12), 1566, doi:10.1029/2001GL014649.

Buffett, B. A. (2003), The thermal state of Earth's core, *Science*, *299*, 1675–1676, doi:10.1126/science.1081518.

Cherniak, D. J. (2002), REE Diffusion in feldspar, *Chem. Geol.*, *193*, 25–41, doi:10.1016/S0009-2541(02)00246-2.

Coe, R. S. (1967), The determination of paleointensities of the Earth's magnetic field with emphasis on mechanisms which could cause non-ideal behavior in Thellier's method, *J. Geomagn. Geoelectr.*, *19*, 157–178.

Coe, R. S., and G. A. Glatzmaier (2006), Symmetry and stability of the geomagnetic field, *Geophys. Res. Lett.*, *33*, L21311, doi:10.1029/2006GL027903.

Cogné, J. P. (1987), TRM deviations in anisotropic assemblages of multidomain magnetite, *Geophys. J. R. Astron. Soc.*, *91*, 1013–1023.

Coogan, L. A., G. R. T. Jenkin, and R. N. Wilson (2002), Constraining the cooling rate of the lower oceanic crust: A new approach applied to the Oman ophiolite, *Earth Planet. Sci. Lett.*, *199*, 127–146, doi:10.1016/S0012-821X(02)00554-X.

Costin, S. O., and S. L. Butler (2006), Modelling the effects of internal heating in the core and lowermost mantle on the earth's magnetic history, *Phys. Earth Planet Inter.*, *157*, 55–71, doi:10.1016/j.pepi.2006.03.009.

DePaolo, D. J., and G. J. Wasserburg (1979), Sm-Nd age of the Stillwater complex and the mantle evolution curve for neodymium, *Geochim. Cosmochim. Acta*, *43*, 999–1008, doi:10.1016/0016-7037(79)90089-9.

Draeger, U., M. Prevot, T. Poidras, and J. Riisager (2006), Single-domain chemical, thermochemical, and thermal remanences in a basaltic rock, *Geophys. J. Int.*, *166*, 12–32, doi:10.1111/j.1365-246X.2006.02862.x.

Dunlop, D. J., and Y. Yu (2004), Intensity and polarity of the field during Precambrian time, in *Timescales of the Paleomagnetic Field*, edited by J. E. T. Channell et al., pp. 85–100, AGU, Washington, D. C.

Feinberg, J. M., H. R. Wenk, P. R. Renne, and G. R. Scott (2004), Epitaxial relationships of clinopyroxene-hosted magnetite determined using electron backscatter diffraction (EBSD) technique, *Am. Mineral.*, *89*, 462–466.

Feinberg, J. M., G. R. Scott, P. R. Renne, and H. R. Wenk (2005), Exsolved magnetite inclusions in silicates: Features determining their remanence behavior, *Geology*, *33*, 513–516, doi:10.1130/G21290.1.

Feinberg, J. M., R. J. Harrison, T. Kasama, R. Dunin-Borkowski, G. R. Scott, and P. R. Renne (2006), Effects of internal mineral structures on the magnetic remanence of silicate-hosted titanomagnetite inclusions: An electron holography study, *J. Geophys. Res.*, *111*, B12S15, doi:10.1029/2006JB004498.

Fenton, M. D., and G. Faure (1969), The age of the igneous rocks of the Stillwater Complex, Montana, *Geol. Soc. Am. Bull.*, *80*, 1599–1604, doi:10.1130/0016-7606(1969)80[1599:TAOTIR]2.0.CO;2.

Fleet, M. E., G. A. Bilcox, and R. L. Barnett (1980), Oriented magnetite inclusions in pyroxenes from the Grenville province, *Can. Mineral.*, *18*, 89–99.

Gee, J. S., W. P. Meurer, P. A. Selkin, and M. J. Cheadle (2004), Quantifying three-dimensional silicate fabrics in cumulates using cumulative distribution functions, *J. Petrol.*, *45*(10), 1983–2009, doi:10.1093/petrology/egh045.

Geissman, J. W., S. S. Harlan, and A. J. Brearley (1988), The physical isolation of carriers of geologically stable remanent magnetization: Paleomagnetic and rock magnetic microanalysis and electron microscopy, *Geophys. Res. Lett.*, *15*, 479–482, doi:10.1029/GL015i005p00479.

Glatzmaier, G. A., R. S. Coe, L. Hongre, and P. H. Roberts (1999), How the Earth's mantle controls the frequency of

geomagnetic reversals, *Nature*, *401*, 885–890, doi:10.1038/44776.

Grove, T. L., M. B. Baker, and R. J. Kinzler (1984), Coupled CaAl-NaSi diffusion in plagioclase feldspar: Experiments and application to cooling rate geospeedometry, *Geochim. Cosmochim. Acta*, *48*, 2113–2121, doi:10.1016/0016-7037(84)90391-0.

Gubbins, D., D. Alfe, G. Masters, G. D. Price, and M. J. Gillan (2003), Can the Earth's dynamo run on heat alone?, *Geophys. J. Int.*, *155*, 609–622, doi:10.1046/j.1365-246X.2003.02064.x.

Hale, C. J. (1987), Paleomagnetic data suggest link between the Archean-Proterozoic boundary and inner-core nucleation, *Nature*, *329*, 233–237, doi:10.1038/329233a0.

Halgedahl, S. L., R. Day, and M. Fuller (1980), The effect of cooling rate on the intensity of weak-field TRM in single-domain magnetite, *J. Geophys. Res.*, *85*(B7), 3690–3698, doi:10.1029/JB085iB07p03690.

Harrison, T. M. (1982), The diffusion of ^{40}Ar in hornblende, *Contrib. Mineral. Petrol.*, *78*, 324–331, doi:10.1007/BF00398927.

Harrison, T. M., I. Duncan, and I. MacDougall (1985), Diffusion of ^{40}Ar in biotite; temperature, pressure and compositional effects, *Geochim. Cosmochim. Acta*, *49*, 2461–2468, doi:10.1016/0016-7037(85)90246-7.

Hartl, P., and L. Tauxe (1997), 11 million years of Oligocene geomagnetic field behaviour, *Geophys. J. Int.*, *128*, 217–229, doi:10.1111/j.1365-246X.1997.tb04082.x.

Hext, G. (1963), The estimation of second-order tensors, with related tests and designs, *Biometrika*, *50*, 353–357.

Hollerbach, R., and C. A. Jones (1993), Influence of the Earth's inner core on geomagnetic fluctuations and reversals, *Nature*, *365*, 541–543, doi:10.1038/365541a0.

Hyodo, H., and D. J. Dunlop (1993), Effect of anisotropy on the paleomagnetic contact test for a Grenville dike, *J. Geophys. Res.*, *98*, 7997–8017, doi:10.1029/92JB02915.

Kistler, R. W., J. D. Obradovich, and E. D. Jackson (1969), Isotopic ages of rocks and minerals from Stillwater Complex, Montana, *J. Geophys. Res.*, *74*, 3226–3227, doi:10.1029/JB074i012p03226.

Kletetschka, G., M. D. Fuller, T. Kohout, P. J. Wasilewski, E. Herrero-Bervera, N. F. Ness, and M. H. Acuna (2006), TRM in low magnetic fields: A minimum field that can be recorded by large multidomain grains, *Phys. Earth Planet Inter.*, *154*, 290–298, doi:10.1016/j.pepi.2005.07.005.

Labotka, T. C., and R. L. Kath (2001), Petrogenesis of the contact-metamorphic rocks beneath the Stillwater Complex, Montana, *Geol. Soc. Am. Bull.*, *113*, 1312–1323, doi:10.1130/0016-7606(2001)113<1312:POTCMR>2.0.CO;2.

Labrosse, S., and M. Macouin (2003), The inner core and the geodynamo, *C. R. Geosci.*, *335*, 37–50, doi:10.1016/S1631-0713(03)00013-0.

Lambert, D. D., D. M. Unruh, and E. C. Simmons (1985), Isotopic investigations of the Stillwater Complex: A review, in *The Stillwater Complex*, *Montana: Geology and Guide*, edited by G. K. Czamanske and M. L. Zientek, pp. 46–54, Mont. Bur. of Mines and Geol., Butte, Mont.

Longhi, J., J. L. Wooden, and K. D. Coppinger (1983), The petrology of high-Mg dikes from the Beartooth Mountains, Montana: A search for the parent magma of the Stillwater Complex, *J. Geophys. Res.*, *88*(S1), B53–B69, doi:10.1029/JB088iS01p00B53.

Manhes, G., C. J. Allègre, B. Dupré, and B. Hamelin (1980), Lead isotope study of basic-ultrabasic layered complexes: Speculations about the age of the earth and primitive mantle

characteristics, *Earth Planet. Sci. Lett.*, *47*, 370–382, doi:10.1016/0012-821X(80)90024-2.

Marcantonio, F., A. Zindler, L. Reisberg, and E. A. Mathez (1993), Re-Os isotopic systematics in chromitites from the Stillwater Complex, Montana, USA, *Geochim. Cosmochim. Acta*, *57*, 4029–4037, doi:10.1016/0016-7037(93)90351-V.

McCallum, I. S. (1996), The Stillwater Complex, in *Layered Intrusions*, edited by R. G. Cawthorn, pp. 441–484, Elsevier, Amsterdam.

Meurer, W. P., and A. E. Boudreau (1996), An evaluation of models of apatite compositional variability using apatite from the Middle Banded Series of the Stillwater Complex, Montana, *Contrib. Mineral. Petrol.*, *125*, 225–236, doi:10.1007/s004100050218.

Meurer, W. P., and M. E. S. Meurer (2006), Using apatite to dispel the "trapped liquid" concept and to understand the loss of interstitial liquid by compaction in mafic cumulates; an example from the Stillwater Complex, Montana, *Contrib. Mineral. Petrol.*, *151*, 187–201, doi:10.1007/s00410-005-0054-3.

Morimoto, C., Y. Otofuji, M. Miki, H. Tanaka, and T. Itaya (1997), Preliminary paleomagnetic results of an Archaean dolerite dike of west Greenland: Geomagnetic field intensity at 2.8 Ga, *Geophys. J. Int.*, *128*, 585–593, doi:10.1111/j.1365-246X.1997.tb05320.x.

Mueller, P. A., and J. L. Wooden (1976), Rb-Sr whole-rock age of the contact aureole of the Stillwater Igneous Complex, Montana, *Earth Planet. Sci. Lett.*, *29*, 384–388, doi:10.1016/0012-821X(76)90143-6.

Nagata, T., Y. Arai, and K. Momose (1963), Secular variation of the geomagnetic total force during the last 5000 years, *J. Geophys. Res.*, *68*, 5277–5282.

Nunes, P. D., and G. R. Tilton (1971), Uranium-lead ages of minerals from the Stillwater Igneous Complex and associated rocks, Montana, *Geol. Soc. Am. Bull.*, *82*, 2231–2250, doi:10.1130/0016-7606(1971)82[2231:UAOMFT]2.0.CO;2.

Page, N., W. Nokleberg, and R. Miller (2002), Geologic map of the Stillwater Complex, Montana: A digital database, *U. S. Geol. Surv. Misc. Geol. Invest. Map, I-797*.

Powell, J. L., W. R. Skinner, and D. Walker (1969), Whole-rock Rb-Sr age of metasedimentary rocks below the Stillwater Complex, Montana, *Geol. Soc. Am. Bull.*, *80*, 1605–1612, doi:10.1130/0016-7606(1969)80[1605:WRAOMR]2.0.CO;2.

Premo, W. R., R. T. Helz, M. L. Zientek, and R. B. Langston (1990), U-Pb and Sm-Nd ages for the Stillwater Complex and its associated sills and dikes, Beartooth Mountains, Montana: Identification of a parent magma?, *Geology*, *18*, 1065–1068, doi:10.1130/0091-7613(1990)018<1065:UP-ASNA>2.3.CO;2.

Pullaiah, G., E. Irving, K. L. Buchan, and D. J. Duhnlop (1975), Magnetization changes caused by burial and uplift, *Earth Planet. Sci. Lett.*, *28*, 133–143, doi:10.1016/0012-821X(75)90221-6.

Raines, G., and B. Johnson (1995), Digital representation of the Montana state geologic map: A contribution to the Interior Columbia River Basin Ecosystem Management Project, *U. S. Geol. Surv. Open File Rep., 1978*, 95–691.

Renne, P. R., G. R. Scott, J. M. G. Glen, and J. M. Feinberg (2002), Oriented inclusions of magnetite in clinopyroxene: Source of stable remanent magnetization in gabbros of the Messum Complex, Namibia, *Geochem. Geophys. Geosyst.*, *3*(12), 1079, doi:10.1029/2002GC000319.

Rice, J. A. (1995), *Mathematical Statistics and Data Analysis*, Duxbury, Belmont, Calif.

Riisager, P., and J. Riisager (2001), Detecting multidomain magnetic grains in Thellier palaeointensity experiments, *Phys. Earth Planet Inter.*, *125*, 111–117, doi:10.1016/S0031-9201(01)00236-9.

Selkin, P. A. (2003), Archean paleointensity from layered intrusions, Ph.D. thesis, 328 pp., Univ. of Calif., San Diego, La Jolla, Calif.

Selkin, P. A., J. S. Gee, L. Tauxe, W. P. Meurer, and A. J. Newell (2000), The effect of remanence anisotropy on paleointensity estimates: A case study from the Archean Stillwater Complex, *Earth Planet. Sci. Lett.*, *183*, 403–416, doi:10.1016/S0012-821X(00)00292-2.

Selkin, P. A., J. S. Gee, and L. Tauxe (2007), Nonlinear thermoremanence acquisition and implications for paleointensity data, *Earth Planet. Sci. Lett.*, *256*, 81–89, doi:10.1016/j.epsl.2007.01.017.

Smirnov, A. V., and J. A. Tarduno (2004), Secular variation of the Late Archean-Early Proterozoic geodynamo, *Geophys. Res. Lett.*, *31*, L16607, doi:10.1029/2004GL020333.

Smirnov, A. V., and J. A. Tarduno (2005), Thermochemical remanent magnetization in Precambrian rocks: Are we sure the geomagnetic field was weak?, *J. Geophys. Res.*, *110*, B06103, doi:10.1029/2004JB003445.

Stephenson, A. (1993), Three-axis static alternating field demagnetization of rocks and the identification of natural remanent magnetization, gyroremanent magnetization, and anisotropy, *J. Geophys. Res.*, *98*, 373–381, doi:10.1029/92JB01849.

Stevenson, D. J. (2003), Planetary magnetic fields, *Earth Planet Sci. Lett.*, *208*, 1–11, doi:10.1016/S0012-821X(02)01126-3.

Stevenson, D. J., T. Spohn, and G. Schubert (1983), Magnetism and thermal evolution of the terrestrial planets, *Icarus*, *54*, 466–489, doi:10.1016/0019-1035(83)90241-5.

Strik, G., T. S. Blake, T. E. Zegers, S. H. White, and C. G. Langereis (2003), Palaeomagnetism of flood basalts in the Pilbara Craton, Western Australia: Late Archaean continental drift and the oldest known reversal of the geomagnetic field, *J. Geophys. Res.*, *108*(B12), 2551, doi:10.1029/2003JB002475.

Tanaka, H., M. Kono, and H. Uchimura (1995), Some global features of paleointensity in geological time, *Geophys. J. Int.*, *120*, 97–102, doi:10.1111/j.1365-246X.1995.tb05913.x.

Tarduno, J. A., R. D. Cottrell, and A. V. Smirnov (2006), The paleomagnetism of single silicate crystals: Recording geomagnetic field strength during mixed polarity intervals, superchrons, and inner core growth, *Rev. Geophys.*, *44*, RG1002, doi:10.1029/2005RG000189.

Tarduno, J. A., R. D. Cottrell, M. K. Watkeys, and D. Bauch (2007), Geomagnetic field strength 3.2 billion years ago recorded by single silicate crystals, *Nature*, *446*, 657–660, doi:10.1038/nature05667.

Tatsumoto, M., and D. Coffrant (1980), Samarium-Neodymium age of the Stillwater Complex, Montana, *U. S. Geol. Surv. Prof. Pap.*, *1175*, 205.

Tauxe, L. (2006), Long-term trends in paleointensity: The contribution of DSDP/ODP submarine basaltic glass collections, *Phys. Earth Planet Inter.*, *156*(3–4), 223–241, doi:10.1016/j.pepi.2005.03.022.

Tauxe, L., C. Constable, C. L. Johnson, A. A. P. Koppers, W. R. Miller, and H. Staudigel (2003), Paleomagnetism of the southewestern USA recorded by 0–5 Ma igneous rocks, *Geochem. Geophys. Geosyst.*, *4*(4), 8802, doi:10.1029/2002GC000343.

Thellier, E., and O. Thellier (1959), Sur l'intensité du champ magnétique terrestre dans le passé historique et géologique, *Ann. Geophys.*, *15*, 285–378.

Thomson, J. A. (2008), Beneath the Stillwater Complex: Petrology and geochemistry of quartz-plagioclase-cordierite (or garnet)-orthopyroxene-biotite ± spiunel hornfels, Mountain View area, Montana, *Am. Mineral.*, *93*, 438–450, doi:10.2138/am.2008.2572.

Wilke, M., and H. Behrens (1999), The dependence of the partitioning of iron and europium between plagioclase and hydrous tonalitic melt on oxygen fugacity, *Contrib. Mineral. Petrol.*, *137*, 102–114, doi:10.1007/s004100050585.

Xu, W., J. W. Geissman, R. van der Voo, and D. R. Peacor (1997), Electron microscopy of iron oxides and implications for the origin of magnetizations and rock magnetic properties of Banded Series rocks of the Stillwater Complex, Montana, *J. Geophys. Res.*, *102*(B6), 12,139–12,157, doi:10.1029/97JB00303.

York, D. (1967), The best isochron, *Earth Planet. Sci. Lett.*, *2*, 479–482, doi:10.1016/0012-821X(67)90193-8.

York, D. (1968), Least squares fitting of a straight line with correlated errors, *Earth Planet. Sci. Lett.*, *5*, 320–324, doi:10.1016/S0012-821X(68)80059-7.

Yoshihara, A., and Y. Hamano (2000), Intensity of the Earth's magnetic field in late Archean obtained from diabase dikes of the Slave Province, Canada, *Phys. Earth Planet Inter.*, *117*, 295–307, doi:10.1016/S0031-9201(99)00103-X.

Yu, Y., and D. Dunlop (2001), Paleointensity determination on the Late Precambrian Tudor Gabbro, Ontario, *J. Geophys. Res.*, *106*(B11), 26,331–26,343, doi:10.1029/2001JB000213.

Yu, Y., and D. J. Dunlop (2003), On partial thermoremanent magnetization tail checks in Thellier paleointensity determination, *J. Geophys. Res.*, *108*(B11), 2523, doi:10.1029/2003JB002420.

Yu, Y., L. Tauxe, and A. Genevey (2004), Toward an optimal geomagnetic field intensity determination technique, *Geochem. Geophys. Geosyst.*, *5*, Q02H07, doi:10.1029/2003GC000630.